Recursive penalized least squares solution for dynamical inverse problems of EEG generation

Okito Yamashita[1], Andreas Galka[2 3] Tohru Ozaki[1 3],

Rolando Biscay[4], Pedro Valdes-Sosa[5]

November 2003

[1] Department of Statistical Science, The Graduate University for Advanced Studies, Minami-Azabu 4-6-7, Tokyo 106-8569, Japan
[2] Institute of Experimental and Applied Physics, University of Kiel, 24098 Kiel, Germany
[3] Institute of Statistical Mathematics (ISM), Minami-Azabu 4-6-7, Tokyo 106-8569, Japan
[4] University of Havana, Ciudad Habana, Calle 34 No.04-2
[5] Cuban Neuroscience Center, Ave 25 No.5202 esquina 158 Cubanacán, POB 6880, 6990, Ciudad Habana, Cuba

Abstract

In this paper we consider the dynamical inverse problem of EEG generation where a specific dynamics for the electrical current distribution is assumed. By casting this problem into a state space representation and assuming a specific class of parametric models for the dynamics, we can impose general spatio-temporal constraints onto the solution. For the purpose of estimating the parameters and evaluating the model, we employ the Akaike Bayesian Information Criterion (ABIC), which is based on the type II likelihood. As a new approach for estimating the current distribution we introduce a method which we call "Dynamic LORETA". A recursive penalized least squares (RPLS) step forms the main element of our implementation. Whereas LORETA exploits exclusively spatial information, Dynamic LORETA exploits both spatial and temporal information, such that it becomes possible to obtain improved inverse solutions. The performance of the new method is evaluated by application to simulated EEG data,

and a considerable improvement over LORETA is found. We also show results for the application to clinical EEG data.

Key words:
dynamical inverse problem, electroencephalogram, distributed source model, Kalman filter, dynamic LORETA, likelihood

1. Introduction

Measurements of electromagnetic fields on the scalp surface provide valuable information about the underlying brain dynamics. By measuring the electrical potential on several locations of the scalp surface, electroencephalograms (EEG) are obtained. It is commonly believed that these potentials are generated by electrical currents in the extracellular media, resulting from the electrical and chemical neuronal activity of the brain.

Currently there is considerable interest in localizing non-invasively such electrical generators of the EEG in the brain. Any inference on these generators, based on EEG measurements, poses an inverse problem. The main difficulty of any attempt to solve this inverse problem arises from the fact that the EEG observations do not contain a sufficient amount of information to precisely reproduce these generators. For this reason, the solution of this inverse problem (i.e. the inverse solution) will be non-unique, since for a given set of EEG measurements there will inevitably be an infinite number of possible inverse solutions which are consistent with the measurements. In order to identify a unique solution, we have to employ additional information in the guise of physiological or physical knowledge about the generators.

In the EEG inverse problem it is a common approach to assume a distributed source model. In this approach, a discretization of brain volume into a set of voxels is employed, each of which is considered to be the location of a current vector. In order to obtain a unique solution, various constraints have been suggested in previous studies: as prominent examples we mention optimal resolution (Backus and Gilbert 1968; Grave de Peralta Menendez et al. 1997; Grave de Peralta Menendez and Gonzalez Andio 1999), L_2 minimum norm (Hämäläinen and Ilmoniemi 1984), L_1 minimum norm (called 'selective minimum norm') (Matsuura and Okabe 1995) and maximum spatial smoothness (called 'low resolution brain electromagnetic tomography', LORETA) (Pascual-Marqui et al. 1994).

In several papers (Pascual-Marqui and Michel 1994; Pascual-Marqui 1999; Grave de Peralta Menendez and Gonzalez Andio 2002) , relative advantages and disadvantages of these approaches have been discussed from a purely spatial point of view; however, these approaches exploit exclusively the information contained in one instantaneous measurement, i.e. the set of voltage measurements obtained from various electrodes at one single instant of time, whereas measurements of the EEG clearly have temporal structure.

Recently, temporal constraints have been taken into consideration for various applications related to inverse problems. For example, in the analysis of electrocardiograms (ECG) an algorithm for solving large-scale least squares problems based on multiple constraints, including explicit spatial and temporal constraints, has been proposed (Brooks et al. 1999). For the reconstruction of current distributions in the EEG inverse problem, or, more generally, the EEG/MEG inverse problem, other algorithms for solving the same large-scale least squares problem as mentioned above have been developed (Schmidt et al. 2001; Schmidt and Louis 2002a,b). Inverse problems arising in the analysis of data obtained by Electrical Impedance Tomography (EIT) and Single Photon Emission Tomography (SPET) have been formulated as state estimation problems (Karjalainen et al. 1997; Kaipio et al. 1999; Vauhkonen et al. 2001) , and the use of Kalman filtering and Kalman smoothing has been suggested for the purpose of obtaining estimates

of the state. Phillips et al. (2002) have suggested to introduce a temporal constraint into the EEG/MEG inverse problem by employing a time window and Gaussian kernels.

The temporal constraints, as used in these studies so far, refer only to the aspect of temporal smoothness. In this paper we would like to consider a more general variant of temporal constraints by regarding time-dependent EEG measurements as reflecting generators which evolve according to some dynamics. This problem is called the "dynamical inverse problem". We will formulate the dynamical inverse problem of EEG generation as a state estimation problem; then it will be possible to explicitly express the spatio-temporal constraints as parts of the system equation within the state space representation. We shall put particular emphasis on exploring the dynamics according to the established procedures of statistical modelling, i.e. by assuming a class of parametric models for the dynamics and comparing these model using some criterion (likelihood principle).

In principle, both state estimation and model comparison could be implemented by employing Kalman filtering; however, due to the high dimensionality of state (corresponding to the high number of voxels), in the case of the EEG inverse problem the direct application of conventional Kalman filtering is impracticable. Instead we will introduce a simple and computationally efficient estimation procedure, which is based on the "recursive penalized least squares" (RPLS) method. Furthermore, we will propose to employ the "Akaike Bayesian Information Criterion" (ABIC) (Akaike 1980a,b) as a statistical criterion not only for estimating the regularization parameter, but also for comparing models. As a result, a new algorithm for estimating inverse solutions from EEG time series will be obtained, which we will refer to as ’Dynamic LORETA’ (DynLORETA), since it will combine the spatial smoothness constraint of the LORETA method with additional dynamical constraints.

The structure of this paper is as follows. In section 2 we will briefly review the forward problem of EEG generation and introduce the dynamical inverse problem, as compared to the instantaneous inverse problem. In section 3, first we will review LORETA and introduce DynLORETA. Then the RPLS method will be introduced as a simple approach to the estimation of generators. In section 4 DynLORETA will be compared with (instantaneous) LORETA by a simulation study; we will also show

the result of applying our method to clinical EEG data. Finally section 5 will contain some concluding discussion.

Throughout this paper, we employ the following notation. The transpose of a matrix A is denoted by A', and a $n \times n$ identity matrix is denoted by I_n. For a vector *x* and a positive definite matrix *C*, we define $\| x \|_C = x' C^{-1} x$. The L_2 norm of a vector *x* is denoted by ||*x*||, corresponding to the case of *C* being an identity matrix.

2. Problem

2.1 Forward problem

The relation between the EEG measurements on the scalp surface and the primary current density resulting from neuronal activity is described by the equation

$$Y = \mathrm{K}\, J + e \,. \tag{1}$$

In Eq.(1) *Y* denotes a vector of length *d* which contains the EEG measurements of scalp electric potential differences at *d* electrodes. $J = (j_1', \cdots j_{N_j}')'$ denotes a vector of length $D=3N_j$ which contains the current density vectors $j_v = (j_{xv}, j_{yv}, j_{zv}), (v = 1, \cdots, N_j)$ at N_j voxels in the brain. The matrix K, linking the current density *J* with the measurement *Y*, is called the lead field matrix. It can be calculated by applying Maxwell's equations to a particular head model (Nunez 1981). The vector e is an additive random element representing unmodeled effects, like observation noise. The forward problem consists of calculating the measurement *Y* from given current density *J*.

2.2 Inverse problem

The inverse problems is defined as the task to estimate the current density *J* from given measurement *Y*. Obviously, it constitutes an ill-posed problem, because the number of electrodes on the scalp is much smaller than the number of voxels for which the current density has to be estimated. Therefore we need to impose additional constraints as prior knowledge. In particular, we call the inverse problem as formulated by Eq.(1) the 'instantaneous inverse problem', because only the measurement at one single time point is used for the estimation of *J*.

An explicit discussion of the definition of 'dynamic(al) inverse problems' first was given by Schmidt and Louis (2002a). According to their definition,

- *the properties J of the examined object do not change during the measuring process. Thus, we have to solve*

$$\mathrm{K}\, J = Y_i \quad \text{for all } i$$

This is called a static inverse problem.

- *the examined object is allowed to change during the measuring process and we have to solve*

$$\mathrm{K}\, J_i = Y_i \quad \text{for all } i$$

This is called a dynamic inverse problem.

Since they used the term 'dynamic inverse problem' for broadly describing any time-varying situation, but without reference to the particular case of variations in time which are the result of an actual dynamical evolution, the term 'nonstationary inverse problem' seems to be more suitable for their definition.

In this paper, the term ’dynamical inverse problem’ is used for a slightly more restricted situation, as defined by:

- Solutions of a ’dynamical inverse problem’ have to be in agreement with a twofold set of restricting information, which is represented by
    - the observation equation for all time points considered

      $Y_t = \mathrm{K}\, J_t + e_t \quad (t = 1,\ 2,\ \cdots)$, and
    - some prespecified dynamics about $J_t, J_{t-1}, J_{t-2}, \cdots$.
- Solutions of an ’instantaneous (static) inverse problem’ have to be in agreement with a twofold set of restricting information, which is represented by
    - the observation equation at one fixed time point $Y = \mathrm{K}\, J + e$, and
    - prior knowledge about *J*.

In our definition, an explicit assumption for the evolution of time course of J_t is imposed, which will simplify the mathematical formulation of the problem, as will be shown in the next section.

In the case of the instantaneous inverse problem, the solution only reflects an instantaneous observation Y_t, whereas in the case of the dynamical inverse problem it reflects a sequence of temporally successive observations $Y_t, Y_{t-1} \cdots$ such that some dynamics of the generators is imposed. In other words, as shown schematically in Fig.1, the dependence of the observation Y_t on the evolution of J_t is explicitly considered in the dynamical inverse problem. If the evolution of J_t does not follow any dynamics, the dynamical inverse problem becomes equivalent to the instantaneous problem, i.e. the dynamical problem is a generalization of the instantaneous problem.

3. Method

3.1 LORETA

LORETA was first suggested by Pascual-Marqui et al. (1994) in order to overcome the incapability of correct localization in 3-dimensional solution spaces which had been observed for the earlier approaches. As prior knowledge LORETA imposes a spatial smoothness constraint onto the solution *J*. This spatial smoothness constraint is expressed by using the (3-dimensionally discretized) Laplacian matrix L as defined by

$$[M]_{ij} = \begin{cases} 6 & (i = j) \\ -1 & (j \text{ is a neighbor of } i) \\ 0 & (\text{otherwise}) \end{cases}$$

$$\mathrm{L} = \frac{1}{6}(M \otimes I_3)$$

The *i*th row vector of L acts as a discrete differentiating operator by forming differences between the nearest neighbors of the *i*th voxel and *i*th voxel itself.

The solution of LORETA is obtained by minimizing a linear mixture of a weighted norm ||L*J*|| and the residuals of the fit according to the observation equation. By assuming a Gaussian distribution $e \sim N(0, s^2 C_e)$ with known covariance structure C_e for the measurement noise in Eq.(1), the objective function of LORETA becomes

$$E(J) = \| Y - \mathrm{K}J \|^2_{C_e} + l^2 \| \mathrm{L}J \|^2, \tag{2}$$

where the parameter l, called the regularization parameter, expresses the balance between fitting the model and the prior constraint of minimizing $\| \mathrm{L}J \|$. The solution of this minimization problem for a given l is obtained by

$$\hat{J} = (\mathrm{K}'C_e^{-1}\mathrm{K} + l^2 \mathrm{L}'\mathrm{L})^{-1} \mathrm{K}'C_e^{-1}Y .$$

3.2 Dynamical LORETA

We shall now present the dynamical LORETA (DynLORETA) approach. For this purpose we will first introduce the appropriate representation of dynamical constraints and then turn to the numerical procedure which provides the inverse solution. Furthermore, the estimation of the regularization parameter and of the parameters of the dynamics will be discussed.

3.2.1 Dynamical constraint

Pioneering work on obtaining dynamical inverse solutions with spatial and temporal smoothness constraints has been presented by Schmidt et al. (2001) for the case of the EEG inverse problem. They formulated the spatial smoothness constraint by using the Laplacian operator and the temporal smoothness constraint by using a time-domain differencing operator. Their temporal smoothness constraint can be interpreted as assuming a random walk model $J_t = J_{t-1} + h_t$ for the dynamics of J_t. For the dynamical model of DynLORETA we will employ a more general class of dynamical constraints, in addition to the spatial smoothness constraint.

At first we define an objective function containing the spatial and temporal smoothness constraints in a similar way as introduced in Schmidt et al. (2001)

$$E(J_t) = \| Y_t - \mathrm{K}\, J_t \|^2_{C_e} + l_1^2 \| \mathrm{L}\, J_t \|^2 + l_2^2 \| \mathrm{L}(J_t - J_{t-1}) \|^2 . \qquad (3)$$

By including the Laplacian matrix *L* into the third term of Eq.(3) interactions between neighboring voxels can also be taken into account. Furthermore this step will reduce considerably the computational expenses, as will be shown in the next subsection.

By introducing a new parameter ϕ, which represents a balance between the second and third terms of Eq.(3), we can combine the two penalty terms and obtain a more compact expression:

$$E(J_t) = \| Y_t - \mathrm{K}\, J_t \|^2_{C_e} + l^2 \| (1-f)\,\mathrm{L}\, J_t + f\,\mathrm{L}(J_t - J_{t-1}) \|^2$$

$$= \| Y_t - \mathrm{K}\, J_t \|^2_{C_e} + l^2 \| \mathrm{L}(J_t - f\, J_{t-1}) \|^2$$

$$= \| Y_t - \mathrm{K}\, J_t \|^2_{C_e} + l^2 \| J_t - f\, J_{t-1} \|^2_{(\mathrm{L}'\mathrm{L})^{-1}} \quad . \tag{4}$$

Note that the objective functions Eq.(3) and (4) are not mathematically equivalent, however we can regard Eq.(4) as a different way of imposing these two kinds of constraints.

Now we shall rewrite this objective function in the form of a statistical model. From Eq.(4) we obtain the state space representation given by

$$\text{observation} : \; Y_t = \mathrm{K}\, J_t + e_t \qquad e_t \sim N(0, s^2 C_e) \tag{5}$$

$$\text{system} : \; J_t = f\, J_{t-1} + h_t \qquad h_t \sim N(0, t^2 (\mathrm{L}'\mathrm{L})^{-1}) \tag{6}$$

Eqs.(5) and (6) represent the observation equation and the system equation, corresponding to the first and second term of Eq.(4), respectively. As an important advantage of state space representations, we note that we can design more general dynamical model by changing the system equation.

For example, we can consider a more complex dynamical model which also includes previous states beyond the first lag and furthermore allows for interactions between generators on different voxels :

$$J_t = \sum_{i=1}^{p} A_i J_{t-i} + h_t \,. \tag{7}$$

where $A_i \;\; (i = 1, \cdots, p)$ are *D*×*D* matrices. Whereas Eq.(6) represents the case of very simple dynamics, by Eq.(7) various more interesting dynamics can be modeled, displaying features like spatial heterogeneity, local neighbor interaction etc. Examples for designing parametric models for such kinds of dynamics will be shown in the section "Results".

Finally the state space representation with a very general dynamics in the system equation will be given by

$$\begin{cases} Y_t = \mathrm{K}\, J_t + e_t & e_t \sim N(0, s^2 C_e) \\ J_t = f_t(J_{t-1}, \cdots, J_{t-p}, S) + h_t & h_t \sim N(0, t^2 (\mathrm{L}'\mathrm{L})^{-1}) \end{cases} \tag{8}$$

where *S* denotes exogenous variables and can model some external force influencing the brain. The function $f_t(\cdot)$ may be specified to be linear, as in the case of Eq.(7), or may be taken as non-linear or time-dependent.

Here three key points should be emphasized. The first is that the covariance structure of the system noise h_t should be given by $(\mathrm{L}'\mathrm{L})^{-1}$. It is expected that spatial smoothness of J_t will be inherited from instantaneous LORETA. The second is that, as stated already, the model is written in a state space representation. In principle, it is possible to perform optimal inference about J_t by employing the Kalman filter or the extended Kalman filter (Jazwinski 1970; Aoki 1987; Kitagawa and Gersh 1996; Durbin and Koopman 2001). The third is that it depends on the analyst what kind of the dynamics will be assumed. Because there are many possible solutions corresponding to different dynamical models, the resulting solutions should be evaluated by some statistical criterion such as ABIC, as mentioned in the introduction.

3.2.2 Approximate Estimation

As already mentioned in the previous section, in principle, we could obtain the estimate of J_t $(t = 1, \cdots, T)$ by using Kalman filtering. In the least squares sense, the filtered estimator $J_{t|t}$ $(t = 1, \cdots, T)$ obtained by Kalman filtering is the best possible estimator based on past and current observations. However, in the case of the 3-dimensional discretized inverse problem the dimension *D* of the state J_t is 3 times the number of voxels (typically several thousand), therefore the practical application of Kalman filtering to such a very high-dimensional state vector will be very demanding (or even impossible) in terms of computational time and memory consumption due to, for example, the need

to compute and store dense matrices of size $D \times D$. In order to overcome this difficulty it is necessary to design suitable approximations of the standard Kalman filtering approach; in Galka et al. (2002) a new approach to spatiotemporal Kalman filtering is presented which renders this high-dimensional filtering problem tractable. In this paper we would like to introduce a different estimation procedure which is very simple and requires only little modifications with respect to instantaneous LORETA. We choose to call it 'recursive penalized least squares solution' (RPLS solution).

For simplicity we shall assume that the function $f_t(\cdot)$ in Eq.(8) is linear and depends only on the states of the generators at the previous time step:

$$f_t(J_{t-1}, \cdots, J_{t-p}, S) = A_t J_{t-1} \tag{9}$$

where A_t denotes a known matrix of size $D \times D$. But here we note that the assumption of linearity is not essential for the RPLS solution.

We will now discuss the practical estimation procedure in detail. An initial estimate (for $t=1$) of the state J_1 can be obtained by any approach for solving the instantaneous inverse problem. For $t=2,3,\cdots,T$, we can obtain an estimate of J_t by recursively solving the penalized least squares problem

$$\hat{J}_t = \arg\min_{J_t} \left\{ \| Y_t - \mathrm{K}\, J_t \|^2_{C_e} + l^2 \| J_t - A_t \hat{J}_{t-1} \|^2_{(\mathrm{L}'\mathrm{L})^{-1}} \right\} \tag{10}$$

where $\hat{J}_{t-1}$ is the estimate obtained in the previous step. The solution of (10) is given by

$$\hat{J}_t = (\mathrm{K}' C_e^{-1} \mathrm{K} + l^2 \mathrm{L}' \mathrm{L})^{-1} (\mathrm{K}' C_e^{-1} Y_t + l^2 \mathrm{L}' \mathrm{L} A_t \hat{J}_{t-1}) \tag{11}$$

However, direct computation of this expression is numerically impracticable due to the need of inverting a large matrix of size $D \times D$; here D is the dimension of the state. Instead, we will now show a convenient way to obtain a numerically more easily accessible solution by appropriate variable transformation. In addition, this transformation will clearly demonstrate the relationship between the RPLS method and Kalman filtering (see Appendix).

We start from the following variable transformations

$$V_t = J_t - A_t \hat{J}_{t-1} \tag{12}$$

$$r_t = Y_t - \mathrm{K} A_t \hat{J}_{t-1} \tag{13}$$

Here V_t and r_t correspond to system noise and innovation (1-step ahead prediction error), respectively. We can rewrite the objective function of Eq.(10) as follows:

$$E(V_t) = \| r_t - \mathrm{K} V_t \|^2_{C_e} + l^2 \| \mathrm{L} V_t \|^2 \tag{14}$$

Then we can obtain an estimate of J_t by

$$\hat{V}_t = T(l) r_t \tag{15}$$

$$\hat{J}_t = A_t \hat{J}_{t-1} + \hat{V}_t \tag{16}$$

where we have defined

$$T(l) = (\mathrm{K}' C_e \mathrm{K} + l^2 \mathrm{L}' \mathrm{L})^{-1} \mathrm{K}' C_e^{-1} \tag{17}$$

$$= \mathrm{L}^{-1} V \mathrm{diag}\left(\frac{s_i}{s_i^2 + l^2} \right) U' C_e^{-1/2} \tag{18}$$

Here, $U, \mathrm{diag}(s_i), V$ are $d \times d$, $d \times d$ and $D \times d$ matrices obtained from the singular value decomposition (SVD) of $C_e^{-1/2} \mathrm{K} \mathrm{L}^{-1}$ (Mardia et al. 1979). The computation of Eq.(18) is not as demanding as the computation of Eq.(11), because in Eq.(18) the large matrix to be inverted does not depend on l, such that this inversion needs only to be carried out once, whereas in Eq.(11) the inversion has to be carried out repeatedly during the process of finding an optimal value of l. A similar remark applies to the SVD of $C_e^{-1/2} \mathrm{K} \mathrm{L}^{-1}$, which also needs to be computed only once, since these three matrices are known.

3.2.3 Estimating regularization parameter l

The regularization parameter l should be chosen in an objective way, because the inverse solution will depend sensitively on this parameter. Various methods, such as the GCV criterion (Wahba 1990) and the L-curve method (Hansen 1992; Hansen 1994) have been employed for this purpose. In this work we propose to employ ABIC (Akaike 1980a,b) for estimating this parameter, because this criterion can be applied not only for selecting the regularization parameter, but also for the purpose of model comparison.

ABIC is defined as

$$\mathrm{ABIC} = -2l^{(II)}(s,t) + 2N,$$

where *N* is the number of the hyperparameters in the model and $l^{(II)}(s,t)$ is the likelihood of the hyperparameters in the context of empirical Bayesian inference, called the type-II log-likelihood. In the case that there are unobservable variables in the model, the type-II likelihood can be obtained by averaging the joint distribution of all variables, both observable and unobservable, over the unobservable variables:

$$l^{(II)}(s,t) = \log \int p(Y_1,\cdots,Y_T,J_1,\cdots,J_T;s,t)\,dJ_1\cdots dJ_T \tag{19}$$

where Y_t are the observable and J_t the unobservable variables; s,t are hyperparameters.

For the dynamical inverse problem it is very difficult to calculate this multiple integral analytically, therefore we will approximate Eq.(19) by the sum of type-II log-likelihoods at each time point, $l_t^{(II)}(s,t)$. Since in the RPLS method we are basing the inference (if interpreted from the Bayesian viewpoint) on $p(r_t \mid V_t;s)$ and $p(V_t;t)$ as likelihood and prior distribution, respectively (compare Eqs.(12) and (13)), the pointwise type-II log-likelihood based on r_t is given by

$$l_t^{(II)}(s,t) = \log \int p(r_t \mid V_t;s)\,p(V_t;t)\,dV_t \ . \tag{20}$$

Then $l^{(II)}(s,t)$ is approximated by the summation of $l_t^{(II)}(s,t)$. This approximation is justified, if the innovations $r_t\,(t=1,\cdots,T)$ are serially independent with respect to their distributions $p(r_t)$.

If $p(r_t|V_t;s)$ and $p(V_t;t)$ are assumed to be Gaussian, we can analytically calculate this integral and obtain (-2) times the pointwise type-II log-likelihood:

$$-2l_t^{(II)}(s,l)=d\log s^2+\sum_{i=1}^{d}\log\frac{s_i^2+l^2}{l^2}+\frac{1}{s^2}\sum_{i=1}^{d}\tilde{r}_{i,t}\,\frac{l^2}{s_i^2+l^2} \tag{21}$$

where $\tilde{r}_{i,t}$ is the *i*th component of the vector $U'C_e^{-1/2}r_t$ (see Appendix for detail). Here we have replaced the hyperparameter t by $l=s/t$. A constant term has been ignored in Eq.(21). Then ABIC can be expressed by

$$\mathrm{ABIC}(s,l)=Td\log s^2+T\sum_{i=1}^{d}\log\frac{s_i^2+l^2}{l^2}+\frac{1}{s^2}\sum_{t=1}^{T}\sum_{i=1}^{d}\tilde{r}_{i,t}\,\frac{l^2}{s_i^2+l^2}+2N. \tag{22}$$

Estimates of $\hat{s}$ and $\hat{l}$ can be obtained by minimizing this expression, and the minimum value of ABIC resulting from this minimization can be employed for model comparison.

In the case of assuming a parametric model for the dynamics, the parameters q of which are unknown, it is necessary to estimate also these parameters. This can be done again by minimizing ABIC, as given by Eq.(22), but now the innovations (1-step prediction errors) r_t depend on these parameters, such that $\mathrm{ABIC}(s,l)$ becomes $\mathrm{ABIC}(s,l,q)$. In our implementation, this optimization is carried out by the simplex method, as provided by the "fminsearch" function of MATLAB.

4. Results

In this section we will present results for a simulation study and for the analysis of real EEG data. For these calculations the following practical settings were chosen:

- The lead field matrix *K* was calculated by using the boundary element method for a three-shell head model (Riera and Fuentes 1998).
- A brain model, derived from the Average Probabilistic MRI Atlas produced by the Montreal Neurological Institute (Mazziotta et al. 1995), was employed.
- The resolution of the voxel discretization was 7 mm, resulting in a total number of 8723 voxels. Generators are assumed to be located only within gray matter, therefore the number of voxels which have to be considered, reduces to 3433.
- The number and locations of EEG electrodes follows the standard 10-20 system.

4.1 Simulation Example

In order to compare the inverse solutions obtained by LORETA and by DynLORETA we will now perform a simulation experiment. For this purpose we generate a time series of *T*=300 observations from a AR(2) model of voxel dynamics, including nearest-neighbor interactions, as described by

$$
\begin{aligned}
&Y_t = \mathrm{K}\, J_t + e_t \\
&J_t = (a_1 I_D + b_1 \mathrm{L}) J_{t-1} + (a_2 I_D + b_2 \mathrm{L}) J_{t-2} + h_t \\
&\mathrm{var}(e_t) = s^2 I_d,\ \mathrm{var}(h_t) = t^2 (\mathrm{L}'\mathrm{L})^{-1},
\end{aligned}
$$

where the parameters are chosen as $(a_1, a_2, b_1, b_2, s, t)$ =(1.82, -1.00, 0.05, 0.00, 0.03, 0.01), and the vectors of initial current densities J_0, J_{-1} are chosen in a way such that two extended sources of activity are created, one in the occipital region and one in the cingulate gyrus. A spatial representation of J_0 is shown in the top-left panel of Fig.3. The EEG observations $Y_1, \cdots, Y_T$ corresponding to the simulated $J_1, \cdots, J_T$ with respect to right-ear mastoid reference, are shown in Fig.2. In the figure a stationary oscillation can be seen at most electrodes, except those located within the frontal region.

From these observations, estimates of sources were calculated using the following three methods and conditions;

- DynLORETA with unknown dynamical parameters and known true initial current vectors (denoted by [D]);
- DynLORETA with unknown dynamical parameter and initial current vectors based on LORETA inverse solutions (denoted by [DL]);
- instantaneous LORETA (denoted by [L]).

For each method the regularization parameter l was estimated both by ABIC and GCV, and the dynamical parameters of the methods [D] and [DL] were estimated by minimizing Eq.(22). The resulting estimates and the corresponding values of ABIC and GCV are shown in Table 1. The results displayed in the table show that estimating l using the ABIC criterion is as good as using the computationally more intensive GCV approach.

In Fig.3 we show for time points t=19 and t=120 the spatial distributions of absolute values of local current vectors for the simulation ("truth") and for the inverse solutions obtained by [D], [DL], and [L]. It can be seen in the figure that [D], [DL] and [L] succeed in reproducing the occipital source of activity, although [L] considerably underestimates the amplitude at the center of this source. On the other hand, [L] completely fails to reproduce the independent source in the cingulate gyrus, which is well reconstructed by [D]; instead, [L] produces spurious activity in the temporal region. For t=120, [DL] also fails to reproduce the source in the cingulate gyrus, which reflects the fact that the estimated dynamics is decaying rapidly (compare the corresponding subfigure in Fig.4).

In Fig.4 the same results are presented for the time domain. Here we show for two specific voxels, chosen from the occipital area and the cingulate gyrus, the corresponding time series of absolute values of current vectors for the simulation ("truth") and for the inverse solutions obtained by [D], [DL], and [L]. It can be seen that the solution by [D] coincides very well with the simulated time series for both voxels; this success is due to using accurate estimates of dynamical parameters (see Table 1). With respect to the

main oscillation, also [DL] could reproduce qualitatively the behavior of the simulated time series for both voxels. The deviations from the simulated time series, however, increases with time; this reflects the use of inaccurate estimates of dynamical parameters. Although [L] to some extent also reproduces oscillations for both voxels, this solution completely fails to reproduce their amplitudes correctly. Furthermore, we note that [L] lacks temporal smoothness, which is a consequence of the incapability of LORETA to discriminate between dynamical noise and observation noise; this weakness of instantaneous inverse solutions has already been noticed by Schmidt et al. (2001).

Now we shall discuss the goodness of the solutions as obtained by the three methods. As can be seen in Table 1, there is a succession of [D], [DL] and [L] with respect to increasing values of ABIC. From the viewpoint of model comparison, this result explicitly shows that the solution of [D] is superior to the solution of [DL], which again is superior to the solution of [L]. Here we want to remark that the value of ABIC can only be employed as a relative measure; the difference of the values between two models has the interpretation of a ratio of probabilities, but the value itself has no meaningful interpretation.

Finally we mention that [DL] provides considerably better inverse solutions as compared to [L], even though there was still an underestimation of amplitudes of true sources, resulting from inaccuracy of the initial state estimates and consequently of the estimated dynamics. This is an important result, since [DL] is applicable to the analysis of real data, in contrast to [D]. But the superior results obtained by [D] indicate that further improvements can be achieved by improving the estimation procedure for the initial state. This will be the subject of future work.

4.2 Real Data Analysis

In Fig.5 a clinical EEG recording is shown, recorded from a healthy child in awake state with closed eyes. At the occipital electrodes O1 and O2 an oscillation is visible which represents the characteristic alpha rhythm. For the analysis of this data set a regional homogeneous AR(2) model is employed, given by

$$Y_t = \mathrm{K}\, J_t + e_t$$
$$J_t^v = \begin{cases} a_1 J_{t-1}^v + a_2 J_{t-2}^v + h_t^v & v \in G \\ b_1 J_{t-1}^v + b_2 J_{t-2}^v + h_t^v & v \notin G \end{cases}$$
$$\mathrm{var}(e_t) = s^2 I_d,\ \mathrm{var}(h_t) = t^2 (\mathrm{L}'\mathrm{L})^{-1}.$$

Here the dynamics within a certain region *G* is assumed to differ from the dynamics within the remaining part of brain. We have chosen the region *G* as a sphere of radius 30mm centered within the occipital lobes; the center was chosen according to the result of a LORETA solution of the same data.

In Fig.6, the time series and periodograms of the *x*,*y*,*z* components of the current vector from a particular voxel inside *G* are shown. In each figure, the time series and periodograms both estimated by LORETA and DynLORETA are plotted. Each component of the time series provided by DynLORETA shows clearer alpha oscillations, as compared to the time series provided by LORETA. In the periodograms, we can also see this difference in the range of the alpha rhythm (around 9Hz). In addition, the time series provided by DynLORETA have higher amplitude, as compared to the time series provided by LORETA; this effect had also been shown in the previous simulation experiment.

Estimation of the dynamical parameters (a_1, a_2, b_1, b_2) by numerical optimization provides the estimates (1.95,-0.99,1.54,-0.56). The parametric power spectrum (p.251 of Shumway (2000)), as obtained from the estimated AR parameters inside *G* displays a peak around 8.3Hz, whereas the power spectrum outside *G* does not display any peak, but just a drop of power towards higher frequencies. The peak at 8.3 Hz falls well within the known range for alpha activity. These results illustrate that by DynLORETA it is possible to make detailed inference about the dynamics of the generators of EEG time series.

In Fig.7, we illustrate for 6 consecutive points of time (with a time shift of 0.0234 seconds) the evolution of the spatial distribution of a component of the current vectors, as estimated by DynLORETA and LORETA. We choose to display the component of the current vectors which corresponds to the radial direction of spherical coordinates, with the origin being located at the center of the head. Both DynLORETA and LORETA solutions provide two main sources which are negatively correlated in the

left and right occipital region. These two sources can be considered to be generators of alpha rhythm (Valdés-Sosa et al. 1992; Rodin and Rodin 1995). However, the solution as obtained by DynLORETA shows much more focused sources in the occipital region, whereas the solution as obtained by LORETA shows spurious activities in other regions, such as the temporal lobes and around the vertex (electrode Cz). Furthermore, the quality of the inverse solutions provided by LORETA and DynLORETA can be assessed by comparing their corresponding values of ABIC, which are 1.76×10^5 and 1.24×10^5, respectively. Comparison of these values of ABIC proves that the solution provided by DynLORETA is superior to the solution provided by LORETA.

5. Discussion

In this paper we have addressed the inverse problem of estimating generators of EEG recordings, with particular emphasis on the use of dynamical constraints. The following issues were discussed:

- We have studied the "dynamical inverse problem" of EEG generation. By formulating the dynamical inverse problem in a state space representation, we can introduce general dynamical constraints into the system equation.
- In principle, the optimum solution of this state estimation problem is given by Kalman filtering and Kalman smoothing; however, due to the high dimensionality of state in the EEG inverse problem, direct application of Kalman filtering is very demanding (or even impossible) in terms of computational time and memory consumption. As an alternative, we have proposed to employ the ’Recursive Penalized Least Squares’ (RPLS) method. A detailed discussion of the relation between the RPLS method and Kalman filtering is given in Appendix A.
- As a practicable approach for finding solutions of the dynamical inverse problem for given data without excessive computational expense we have introduced a suitable method which we have called ’Dynamical LORETA’ (DynLORETA), since it is derived from the LORETA method for

solving the instantaneous problem. It is a crucial advantage of DynLORETA that by suitable choice of the system noise covariance structure it inherits from LORETA the desirable feature of maximum spatial smoothness.

- On a PC with a clock rate of 2GHz the computation of DynLORETA for an EEG data set of length T=500 takes a few hours, including optimization of several hyperparameters. In contrast, for the same data set the computation of LORETA takes only a few seconds, including optimization of the regularization parameter. This difference results from the higher number of hyperparameters to be optimized in DynLORETA, as well as the need to perform for each time point t several additional multiplications and summations of high-dimensional matrices within the state space framework. In order to obtain inverse solutions of improved quality, such price in terms of high computational expense has to be paid.
- For the purpose of estimating the hyperparameters, especially the regularization parameter, we have proposed to employ the Akaike Bayesian Information Criterion (ABIC). In a simulation study it was found that ABIC and the Generalized Cross-Validation (GCV) criterion provide similar estimates. Furthermore the value of ABIC can be employed for the purpose of model comparison, because it can be interpreted as the goodness of the fit of the model to the data. We would like to remark that ABIC is a relative measure; while the value of ABIC itself has no meaning, the difference of ABIC between models can be used to evaluate the models.
- As a parametric model for the spatio-temporal brain dynamics to be used in the simulation study, we have employed a AR(2) model including nearest-neighbor interaction. This particular class of parametric models is expected to be useful for two reasons: firstly, these models can be interpreted as discretizations of partial differential equations describing spatio-temporal dynamical phenomena (Smith 1985); secondly, they can be formulated by using highly sparse matrices which renders them appropriate for application to high-dimensional problems.
- In the simulation study we were able to demonstrate superior performance of DynLORETA as compared to LORETA when applied to data generated by dynamically evolving sources. However,

this success depends essentially on the availability of basic information about the underlying dynamics, namely about the form and parameters of the dynamical model. In addition, an important point for achieving substantial improvements of the inverse solutions is given by better estimates of initial states of the RPLS method.

- In an analysis of clinical EEG data we have employed a regional AR(2) model, characterized by the presence of different dynamics inside and outside the occipital area. As a result of DynLORETA we have observed two occipital sources which are negatively correlated. Both from the parameter estimates and from the estimated time series at occipital voxels we could identify oscillations corresponding to alpha rhythm.
- The main advantage of the solutions provided by DynLORETA is given by the fact that their temporal structure results explicitly from a dynamical model. While the spatial features of the LORETA solutions are inherited, additional improvements of the solution become possible through incorporation of temporal information. On the other hand, if the dynamical model has not been well-chosen, the solutions of DynLORETA tend to be very similar to the corresponding LORETA solutions, because inappropriate dynamical constraints result in very weak regularization.

The ideas and methods presented in this paper should be developed further, starting from the following suggestions:

- Information from other brain-imaging modalities (such as fMRI, NIRS) should be incorporated into the estimation task. This will render it possible to explore physiologically more meaningful dynamics and ultimately also result in better inverse solutions.
- Suitable approaches for dimension reduction should be applied to the dynamical states. If this can be accomplished, direct application of Kalman filtering will become feasible.
- More accurate estimation procedures should be developed. The RPLS method can be interpreted as an approximation of Kalman filtering, but it still represents a rough approximation. Therefore

it would be desirable to construct computationally efficient estimation procedures which approach Kalman filtering more closely even in the case of high dimensional states.

Appendix A: The relation between RPLS method and Kalman filtering

The estimation procedure of the RPLS method has the same structure as known from Kalman filtering: first the innovation is calculated (Eq.(13)) using the previous estimate (i.e. forming a prediction) and the current observation, then V_t is calculated (Eq.(15), corresponding to filtering) from the innovation. Let $J_{t\text{-}1|t\text{-}1}$ and $V_{t\text{-}1|t\text{-}1}$ denote the filtered state estimate and the filtered state error variance, respectively, as provided by Kalman filtering at time t-1. At time t a new observation Y_t becomes available, and the state estimate is updated according to

$$J_{t|t} = A_t J_{t-1|t-1} + \boldsymbol{k}\, r_t^k \tag{23}$$

$$\boldsymbol{k} = \left\{ \mathrm{K}' C_e \mathrm{K} + (s^2 c_{t-1} A_t P_{t-1} A_t' + l^{-2} (\mathrm{L}' \mathrm{L})^{-1})^{-1} \right\}^{-1} \mathrm{K}' C_e^{-1} \tag{24}$$

where $\boldsymbol{k}$ denotes the Kalman gain, and the innovation r_t^k is defined by $r_t^k = Y_t - \mathrm{K} A_t J_{t-1|t-1}$. Here we denote the filtered error variance by $V_{t\text{-}1|t\text{-}1}=c_{t\text{-}1}P_{t\text{-}1}$. In the RPLS method, the equation corresponding to Eq.(23) is Eq.(16). Obviously, in Kalman filtering $\boldsymbol{k}\, r_t^k$ is the estimator of system noise; the corresponding estimator is given by Eq.(15). By comparison with Eq.(17) it can readily be seen that the RPLS method becomes consistent with Kalman filtering if $c_{t\text{-}1}\to 0$. While, according to Eq.(24), the Kalman gain essentially depends on three components, representing system noise variance, observation noise variance and the uncertainty of the previous estimate, the RPLS method explicitly depends on only two of these components, namely system noise variance and observation noise variance. In this sense Kalman filtering can be regarded as a more general algorithm than the RPLS method.

Appendix B: The calculation of type II log-likelihood for LORETA

The detailed calculation of type II log-likelihood for LORETA is shown here. We can obtain the approximated type II log-likelihood for DynLORETA, as shown in section "Method", in the same way, by replacing Y_t by r_t in Eq.(13).

From the view of Bayesian inference, the LORETA solution can be interpreted as Maximum A Posteriori (MAP) solution with respect to likelihood and prior distribution, respectively:

$$p(Y_t \mid J_t; s) \sim N(\mathrm{K} J_t, s^2 C_e) \tag{25}$$

$$p(J_t; t) \sim N(0, t^2 (\mathrm{L}'\mathrm{L})^{-1}) \tag{26}$$

Then the type II log-likelihood of one fixed point of time, defined by

$$l_t^{(II)}(s, t) = \log \int p(Y_t \mid J_t; s)\, p(J_t; t)\, dJ_t \tag{27}$$

can be simplified as

$$\begin{aligned} p(Y_t \mid J_t; s)\, p(J_t; t) &= (2p)^{-\frac{d+D}{2}} \mid s^2 C_e \mid^{-\frac{1}{2}} \mid t^2 (\mathrm{L}'\mathrm{L})^{-1} \mid^{-\frac{1}{2}} \exp\left\{-\frac{1}{2s^2} E(J_t; l)\right\} \\ &= (2p)^{-\frac{d+D}{2}} \mid s^2 C_e \mid^{-\frac{1}{2}} \mid t^2 (\mathrm{L}'\mathrm{L})^{-1} \mid^{-\frac{1}{2}} \exp\left\{-\frac{1}{2s^2} E(\hat{J}_t; l)\right\} \\ &\quad \times \exp\left\{-\frac{1}{2s^2} (J_t - \hat{J}_t)' U(l) (J_t - \hat{J}_t)\right\}, \end{aligned} \tag{28}$$

where

$$\begin{aligned} E(J_t; l) &\equiv \| Y_t - \mathrm{K} J_t \|_{C_e}^2 + l^2 \| \mathrm{L} J_t \|^2 \\ \hat{J}_t &\equiv (\mathrm{K}' C_e \mathrm{K} + l^2 \mathrm{L}' \mathrm{L})^{-1} \mathrm{K}' C_e^{-1} Y_t \\ U(l) &\equiv \mathrm{K}' C_e \mathrm{K} + l^2 \mathrm{L}' \mathrm{L} \end{aligned}$$

and $l \equiv \frac{s}{t}$.

Since only the second exponential in Eq.(28) contains the integrand J_t, the integral can be evaluated in closed form as

$$\int p(Y_t \mid J_t; s)\, p(J_t; t)\, dJ_t = (2p)^{-\frac{d}{2}} \mid s^2 C_e \mid^{-\frac{1}{2}} \mid t^2 (\mathrm{L}'\mathrm{L})^{-1} \mid^{-\frac{1}{2}} \mid s^2 U (l)^{-1} \mid^{\frac{1}{2}} \times \exp\left\{ -\frac{1}{2s^2} E(\hat{J}_t; l) \right\}.$$

Then we obtain (-2) times type II log-likelihood as follows:

$$-2 l_t^{(II)}(s, l) = \log \mid s^2 C_e \mid + \frac{1}{s^2} E(\hat{J}_t; l) + \log \frac{\mid t^2 (\mathrm{L}'\mathrm{L})^{-1} \mid}{\mid s^2 U (l)^{-1} \mid}. \tag{29}$$

Here we have replaced the parameter t by $l = s/t$ and constant terms have been ignored. The second and third terms of Eq.(29) can be further simplified by means of the singular value decomposition of $\bar{\mathrm{K}} \equiv C_e^{-1/2} \mathrm{K}\, \mathrm{L}^{-1} = USV'$. The second term can be arranged as

$$\begin{aligned} E(\hat{J}_t; l) &= \| \{ I - \bar{\mathrm{K}} (\bar{\mathrm{K}}' \bar{\mathrm{K}} + l^2 I)^{-1} \bar{\mathrm{K}}' \} C_e^{-\frac{1}{2}} Y_t \|^2 + l^2 \| (\bar{\mathrm{K}}' \bar{\mathrm{K}} + l^2 I)^{-1} \bar{\mathrm{K}}' C_e^{-\frac{1}{2}} Y_t \|^2 \\ &= \| U \{ I - S(S'S + l^2 I)^{-1} S' \} \tilde{Y}_t \|^2 + l^2 \| V (S'S + l^2 I)^{-1} S' \tilde{Y}_t \|^2 \\ &= \tilde{Y}_t' \mathrm{diag}\left(\frac{l^2}{s_i^2 + l^2} \right) \tilde{Y}_t \end{aligned} \tag{30}$$

where $\tilde{Y}_t = U' C_e^{-1/2} Y_t$, and s_i is the ith singular value in the matrix S. The third term can be simplified as

$$\begin{aligned} \log \frac{\mid (\mathrm{L}'\mathrm{L})^{-1} \mid}{\mid l^2 (\mathrm{K}' C_e \mathrm{K} + l^2 \mathrm{L}' \mathrm{L})^{-1} \mid} &= -\log \mid l^2 (\bar{\mathrm{K}}' \bar{\mathrm{K}} + l^2 I)^{-1} \mid \\ &= -\log \mid l^2 (S'S + l^2 I)^{-1} \mid \\ &= \sum_{i=1}^{d} \log \frac{s_i^2 + l^2}{l^2} \end{aligned} \tag{31}$$

Substituting Eqs.(30) and (31) into (29), we can finally obtain (-2) times type II log-likelikhood as

$$-2l_t^{(II)}(s\,,l) = d\log s^{\,2} + \sum_{i=1}^{d}\log\frac{s_i^2 + l^{\,2}}{l^{\,2}} + \frac{1}{s^{\,2}}\sum_{i=1}^{d}\tilde{y}_{i,t}\frac{l^{\,2}}{s_i^2 + l^{\,2}}$$

where $\tilde{y}_{i,t}$ is *i*th component of the vector $\overline{Y}_t$. The hyperparameters $s\,, l$ can be obtained in such way that the function $-2l_t^{(II)}$ will be minimized. Differentiating $-2l_t^{(II)}$ with respect to $s^{\,2}$, the estimate of $s^{\,2}$ is provided by

$$\hat{s^{\,2}} = \frac{1}{d}\sum_{i=1}^{d}\tilde{y}_{i,t}\frac{l^{\,2}}{s_i^2 + l^{\,2}}\,.$$

The regularization parameter l can be obtained by minimizing

$$-2l_t^{(II)}(l) = d\log\hat{s^{\,2}} + d + \sum_{i=1}^{d}\log\frac{s_i^2 + l^{\,2}}{l^{\,2}}\,.$$

Since in the case of LORETA the probability densities $p(Y_t, J_t; s\,, t\,), t = 1,\cdots, T$ are serially independent, the (-2) type II log-likelihood based on *T* data points can be obtained as follows:

$$\begin{aligned}
-2l^{(II)}(s\,,l) &= -2\log\int p(Y_1,\cdots,Y_T, J_1,\cdots, J_T; s\,, t\,)dJ_1\cdots dJ_T \\
&= -2\sum_{t=1}^{T}\log\int p(Y_t\,|\,J_t;\,s\,)P(\,J_t;\,t\,)dJ_t \\
&= Td\log s^{\,2} + T\sum_{i=1}^{d}\log\frac{s_i^2 + l^{\,2}}{l^{\,2}} + \frac{1}{s^{\,2}}\sum_{t=1}^{T}\sum_{i=1}^{d}\tilde{y}_{i,t}\frac{l^{\,2}}{s_i^2 + l^{\,2}}.
\end{aligned}$$

Acknowledgement

This research was supported by the Japan Society for the Promotion of Science (JSPS) through grant 13654075. The work of AG was supported by the Deutsche Forschungsgemeinschaft (DFG) through project GA 673/1-1 and by JSPS through fellowship ID No. P 03059. The authors express their gratitude to Eduardo Martinez-Montes and Nelson Trujillo-Barreto for helpful discussions. Clinical EEG data

was kindly provided by U. Stephani and H. Muhle from the Neuropediatric Hospital of the University of Kiel, Germany.

References

H. Akaike 1980a, Likelihood and the Bayesian procedure. In J. M. Bernardo, M. H. Degroot, D. V. Lindley, and A. F. M. Smith, editors, *Bayesian Statistics*, pages 141–166. Valencia, Spain: University Press.

H. Akaike (1980b), Seasonal adjustment by a Bayesian modeling. *Journal of Time Series Analysis*, 1(1): 1–13.

M. Aoki 1987, *State Space Modeling of Time Series*. Berlin: Springer.

G. Backus and F. Gilbert (1968), The resolving power of gross earth data. *Geophys. J. R. Astr. Soc.*, 16: 169–205.

D. H. Brooks, F. Ghandi, R. S. Macleod, and M. Maratos (1999), Inverse electrocardiography by simultaneous imposition of multiple constraints. *IEEE Transactions on Biomedical Engineering*, 46(1): 3–17.

J. Durbin and S. J. Koopman 2001, *Time Series Analysis by State Space Models*. Oxford Univ. Press.

A. Galka, T. Ozaki, O. Yamashita, R. Biscay, and P. Valdes-Sosa (2002), A solution to the dynamical inverse problem of EEG generation using spatiotemporal Kalman filtering. Research Memorandum 862, The Institute of Statistical Mathematics.

R. Grave de Peralta Menendez and S. L. Gonzalez Andio (1999), Backus and gilbert method for vector fields. *Human Brain Mapping*, 7: 161–165.

R. Grave de Peralta Menendez and S. L. Gonzalez Andio (2002), Comparison of algorithms for localization of focal source evaluation with simulated data and analysis of experimental data. *International Journal of Bioelectromagnetism*, 4(1).

R. Grave de Peralta Menendez, O. Hauk, S. L. Gonzalez Andio, H. Vogt, and C. Michel (1997), Linear inverse solutions with optimal resolution kernels applied to electromagnetic tomography. *Human Brain Mapping*, 5: 454–467.

M. S. Hämäläinen and R. J. Ilmoniemi (1984), Interpreting measured magnetic fields of the brain: estimates of current distributions. Technical Report TKK-F-A559, Helsinki University of Technology.

P. C. Hansen (1992), Analysis of discrete ill-posed problems by means of the L-curve. *SIAM Review*, 34: 561–580.

P. C. Hansen (1994), Regularization tools: A Matlab package for analysis and solution of discrete ill-posed problems. *Numerical Algorithms*, 6: 1–35.

A. H. Jazwinski 1970, *Stochastic Processes and Filtering Theory*. San Diego: Academic Press.

J. P. Kaipio, P. A. Karjalainen, E. Somersalo, and M. Vauhkonen (1999), State estimation in time-varying electrical impedance tomography. *Annals New York Acad Sci*, 873: 430–439.

P. A. Karjalainen, M. Vauhkonen, and J. P. Kaipio (1997), Dynamic reconstruction in spet. In *Proc. 19th Int. Conf. IEEE Eng. Med. Biol. Society.*

G. Kitagawa and W. Gersh 1996, *Smoothness Priors Analysis of Time Series*. New York: Springer.

K.V. Mardia, J. T. Kent, and J. M. Bibby 1979, *Multivariate Analysis*. San Diego: Academic Press.

K. Matsuura and Y. Okabe (1995), Selective minimum-norm solution of the biomagnetic inverse problem. *IEEE Transactions on Biomedical Engineering*, 42(6): 608–615.

J. C. Mazziotta, A. Toga, A. C. Evans, P. Fox, and J. Lancaster (1995), A probabilistic atlas of the human brain: theory and rationale for its development. *NeuroImage*, 2: 89–101.

P. Nunez 1981, *Electric Fields of the Brain*. New York: Oxford Univ. Press.

R. D. Pascual-Marqui (1999), Review of methods for solving the EEG inverse problem. *International Journal of Bioelectromagnetism*, 1(1): 75–86.

R. D. Pascual-Marqui and C. M. Michel 1994, LORETA: New authentic 3D functional images of the brain. In W. Skandies, editor, *ISBET newsletter*.

R. D. Pascual-Marqui, C. M. Michel, and D. Lehmann (1994), Low resolution electromagnetic tomography: a new method for localizing electrical activity in the brain. *Int. J. Psychophysiol.*, 18: 49–65.

C. Phillips, M. D. Rug, and K. J. Friston (2002), Systematic regularization of linear inverse solutions of the EEG source localization problem. *NeuroImage*, 17: 287–301.

J. J. Riera and M. E. Fuentes (1998), Electric lead field for a piecewise homogeneous volume conductor model of the head. *IEEE Transactions on Biomedical Engineering*, 45(6): 746–753.

E. A. Rodin and M. J. Rodin (1995), Dipole sources of the human alpha rhythm. *Brain Topography*, 7: 201–208.

U. Schmidt and A. K. Louis (2002a), Efficient algorithms for the regularization of dynamic inverse problems: I. theory. *Inverse Problems*, 18: 645–658.

U. Schmidt and A. K. Louis (2002b), Efficient algorithms for the regularization of dynamic inverse problems: II. applications. *Inverse Problems*, 18: 659–676.

U. Schmidt, A. K. Louis, F. Darvas, H. Buchner, and M. Fuchs (2001), Numerical aspects of spatio-temporal current density reconstruction from EEG-/ MEG-data. *IEEE Trans. Med. Imaging*, 20: 314–324.

R. H. Shumway 2000, *Time series analysis and its applications*. New York: Springer.

G. D. Smith 1985, *Numerical solution of partial differential equations: Finite difference methods*. Oxford Univ. Press, 3rd edition.

P. Valdés-Sosa, J. Bosch, R. Grave de Peralta-Menendez, J. L. Hernández, R. Pascual, and R. Biscay (1992), Frequency domain models for the EEG. *Brain Topography*, 4: 309–319.

P. J. Vauhkonen, M. Vouhkonen, and J. P. Kaipio (2001), Fixed-lag smoothing in electrical impedance tomography. *Int. J. Num. Meth. Eng.*, 50: 2195–2209.

G. Wahba 1990, *Spline Models for Observational Data*. Pennsylvania: Society for Industrial and Applied Mathematics.

6. Tables

	DynLORETA [D]	DynLORETA [DL]	LORETA [L]
λ_{GCV}	0.256	0.095	0.0076
λ_{ABIC}	0.259	0.100	0.0065
GCV	2.58×10^{-6}	2.69×10^{-6}	3.71×10^{-6}
ABIC	-4.18×10^{4}	-3.95×10^{4}	-3.56×10^{4}
$(\hat{a}_1, \hat{a}_2, \hat{b}_1, \hat{b}_2)$	(1.82, -1.00, 0.06, 0.008)	(1.87,-1.05,-0.57,0.58)	•

Table 1: Estimates of regularization parameter l and dynamical parameters, and corresponding values of ABIC and GCV for the simulation data. These values are obtained by DynLORETA with known initial states [D], DynLORETA with estimated initial states [DL], and LORETA [L]

7. Figures Captions

Figure 1: Schematic comparison between the instantaneous inverse problem (top) and the dynamical inverse problem (bottom). Sources within brain and EEG observations are represented by rectangles and circles, respectively. Arrows represent the flow of information, as assumed by the underlying model; see section "Problem" for a detailed discussion.

Figure 2: Simulated EEG observations at 19 standard electrode positions of the 10/20-system versus simulation time, according to the model given by Eq.(23).

Figure 3: Spatial distributions of absolute values of local current vectors for the simulation (TRUE) and for the inverse solutions obtained by DynLORETA with known initial state [D], by DynLORETA with unknown initial state [DL] and by LORETA [L]. In the top left panel the initial state of the simulation is shown. Middle and right columns show the inverse solutions at time points t=19 and t=120, respectively. Note that color scale of [L] is different from the color scale of the other three rows.

Figure 4: Time series of absolute values of local current vectors at 2 individual voxels, one chosen from the occipital area (left column) and one from cingulate gyrus (right column), versus simulation time. From top row to bottom row, simulated time series and results for the inverse solutions obtained by DynLORETA with known initial state [D], by DynLORETA with unknown initial state [DL] and by LORETA [L] are shown.

Figure 5: Clinical EEG recording at 19 standard positions of the 10/20-system versus time, obtained from a healthy 8-years old male child, awake with closed eyes. The vertical axis represents observed voltages relative to the average reference.

Figure 6: Time series of the *x*,*y*,*z* components of the estimated local current vector at one voxel, chosen from G (occipital area) (top row of panels) and corresponding periodograms (bottom row of panels) for inverse solutions obtained from the EEG data set shown in Fig.5. Thin lines refer to DynLORETA, and thick lines refer to LORETA.

Figure 7: Spatial distributions of the component of the current vectors corresponding to the radial direction of spherical coordinates for inverse solutions obtained from the EEG data set shown in Fig.5. Upper 6 figures show the solutions as estimated by DynLORETA, and lower 6 figures show the solutions as estimated by LORETA, both at 6 consecutive points in time.

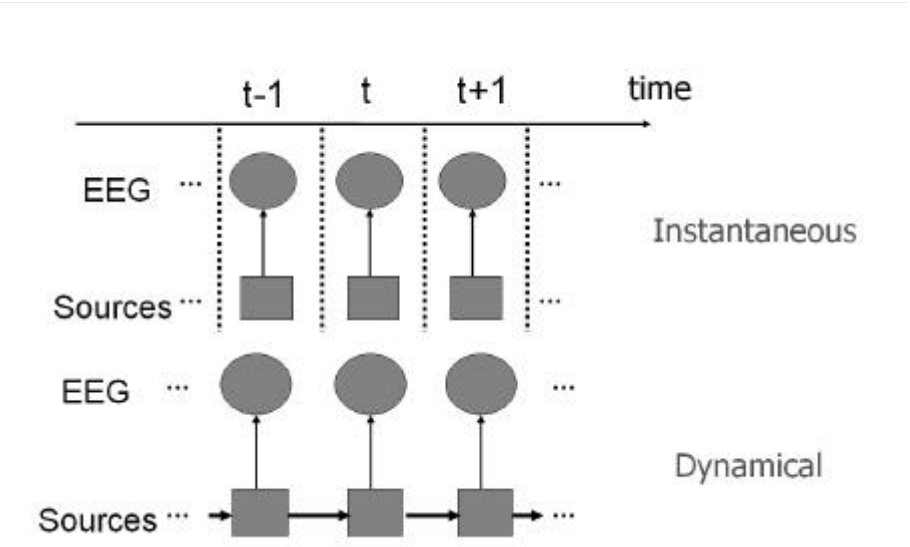
t-1
t
t+1
time
EEG
Sources
Instantaneous
EEG
Sources
Dynamical

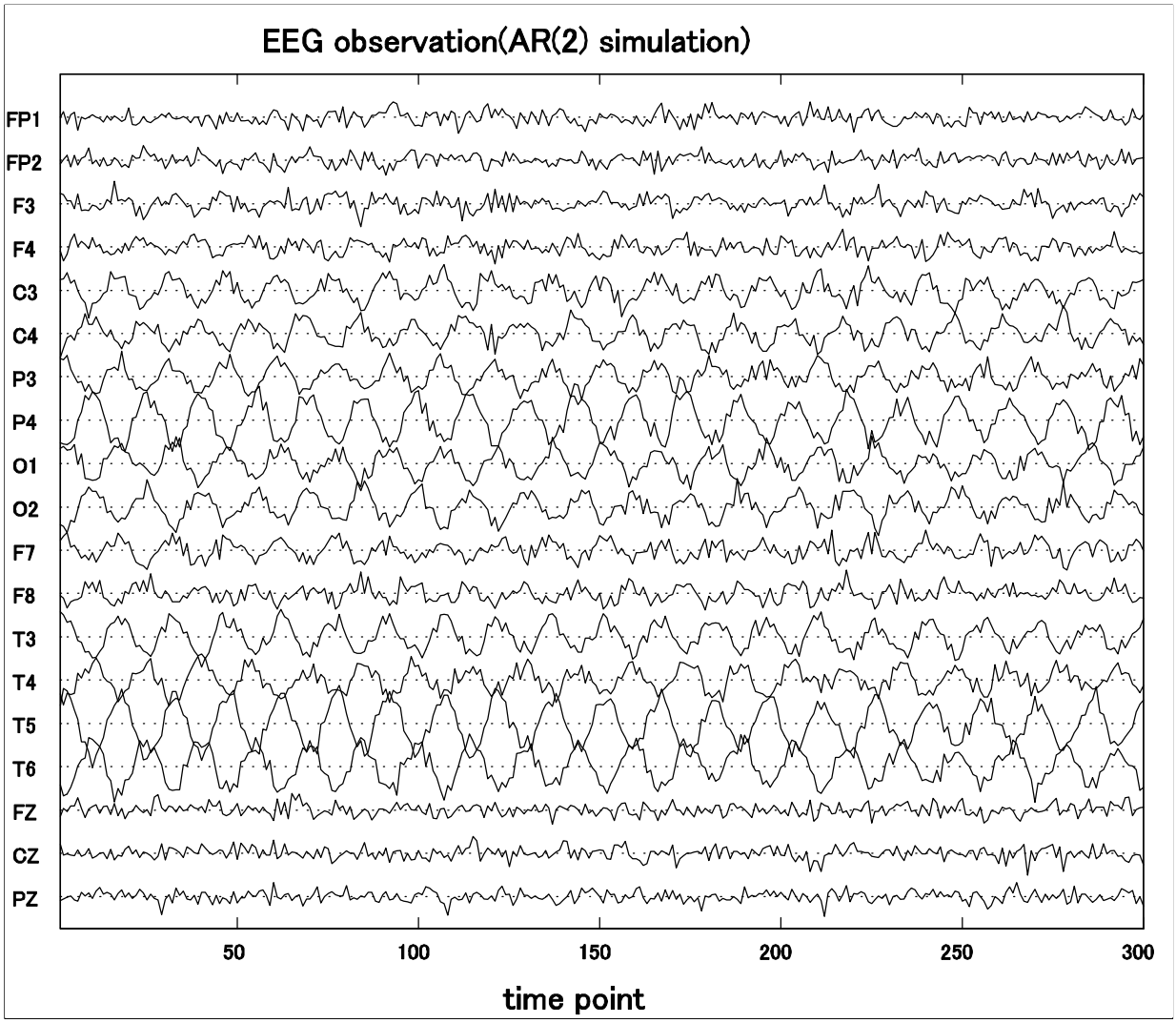
EEG observation(AR(2) simulation)
FP1
FP2
F3
F4
C3
C4
P3
P4
O1
O2
F7
F8
T3
T4
T5
T6
FZ
CZ
PZ
50
100
150
200
250
300
time point

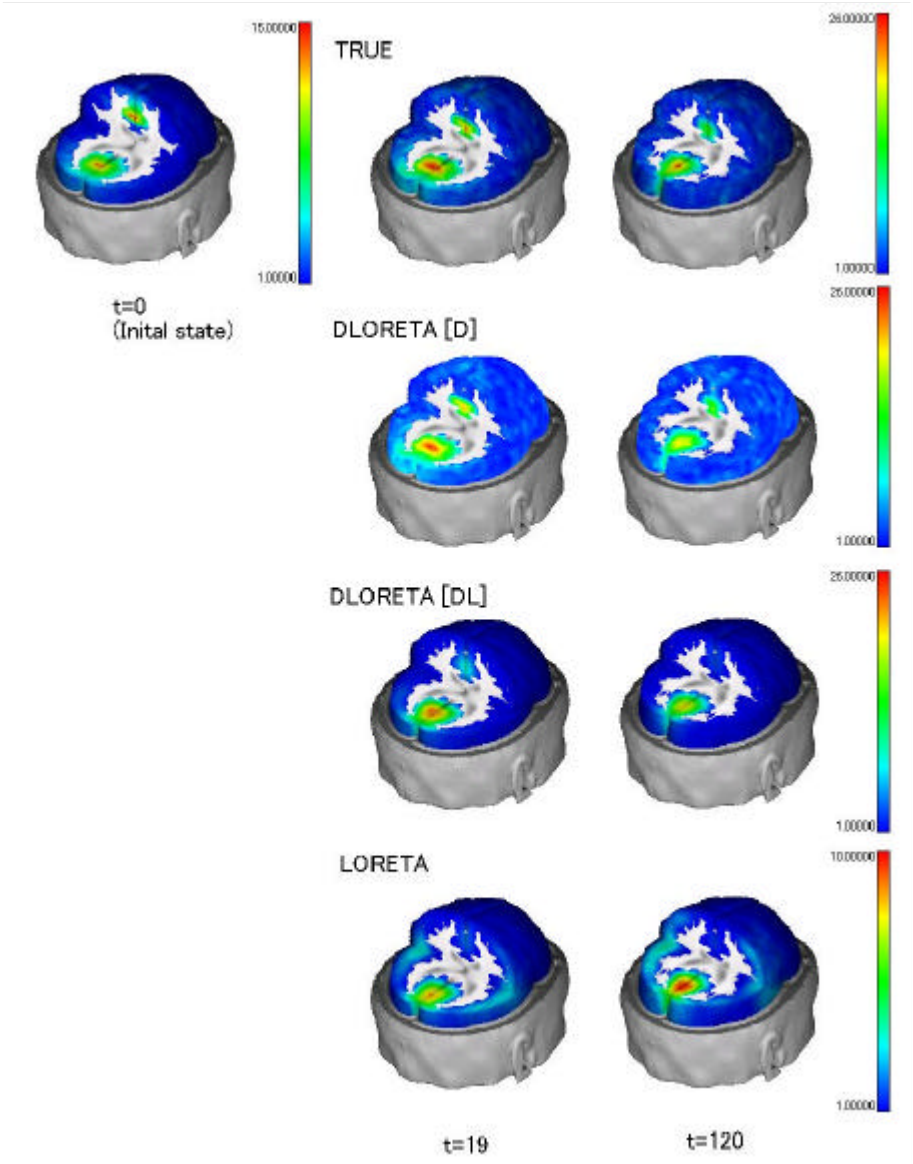
15.00000
1.00000
TRUE
26.00000
1.00000
t=0
(Inital state)
DLORETA [D]
26.00000
1.00000
DLORETA [DL]
26.00000
1.00000
LORETA
10.00000
1.00000
t=19
t=120

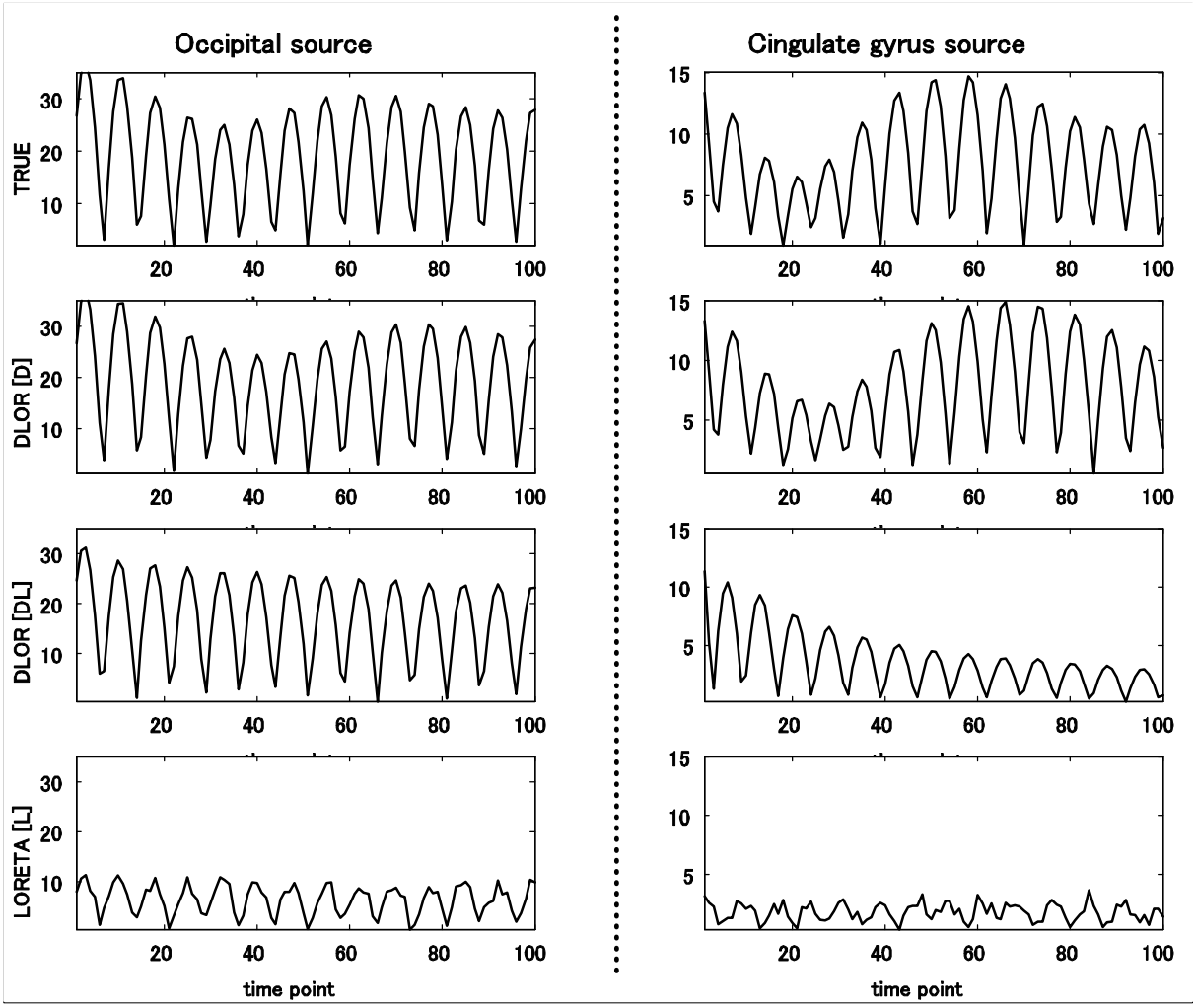
Occipital source
Cingulate gyrus source
TRUE
DLOR [D]
DLOR [DL]
LORETA [L]
time point
time point

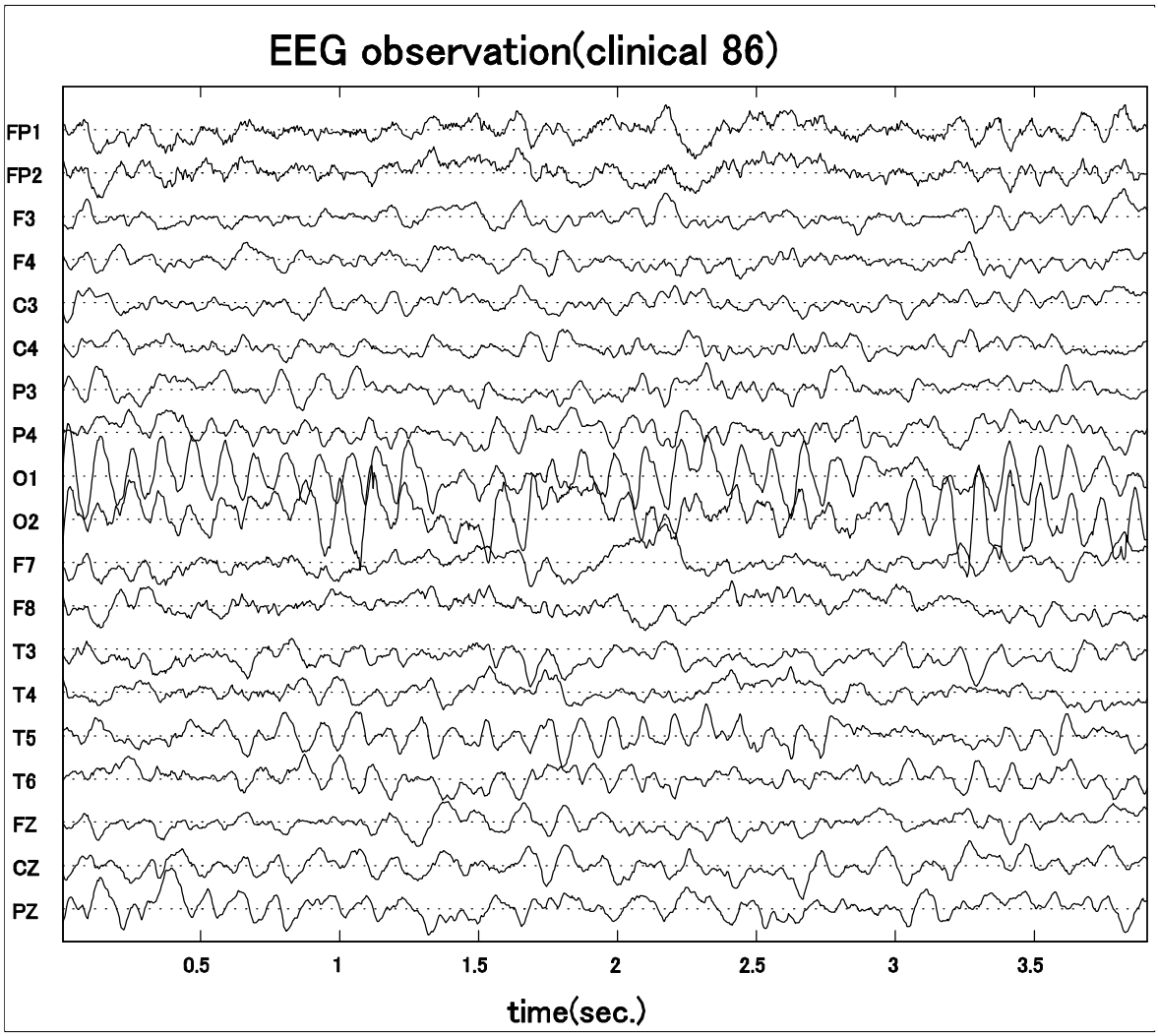
EEG observation(clinical 86)
FP1
FP2
F3
F4
C3
C4
P3
P4
O1
O2
F7
F8
T3
T4
T5
T6
FZ
CZ
PZ
0.5
1
1.5
2
2.5
3
3.5
time(sec.)

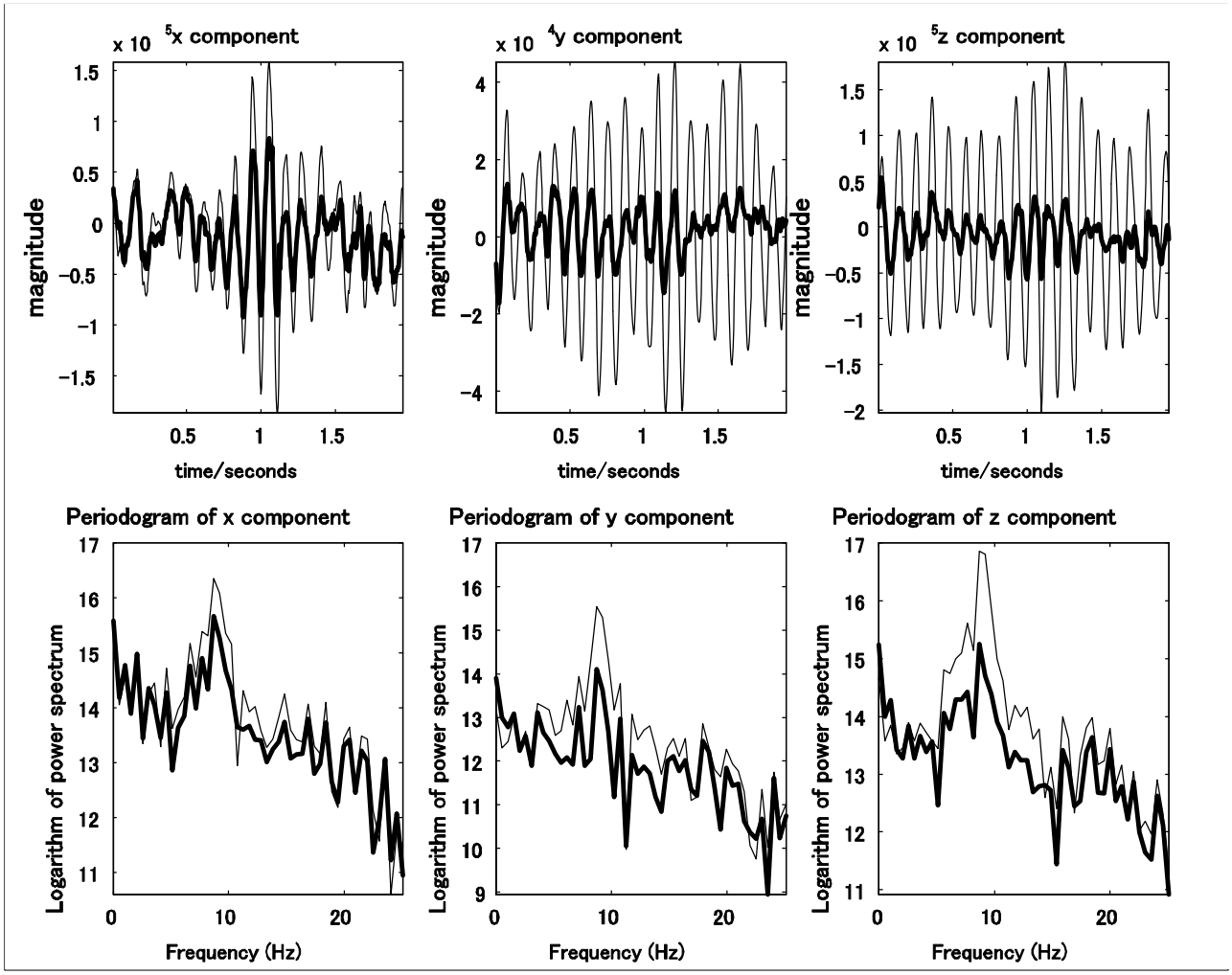
x 10^5 x component
magnitude
time/seconds
x 10^4 y component
magnitude
time/seconds
x 10^5 z component
magnitude
time/seconds
Periodogram of x component
Logarithm of power spectrum
Frequency (Hz)
Periodogram of y component
Logarithm of power spectrum
Frequency (Hz)
Periodogram of z component
Logarithm of power spectrum
Frequency (Hz)

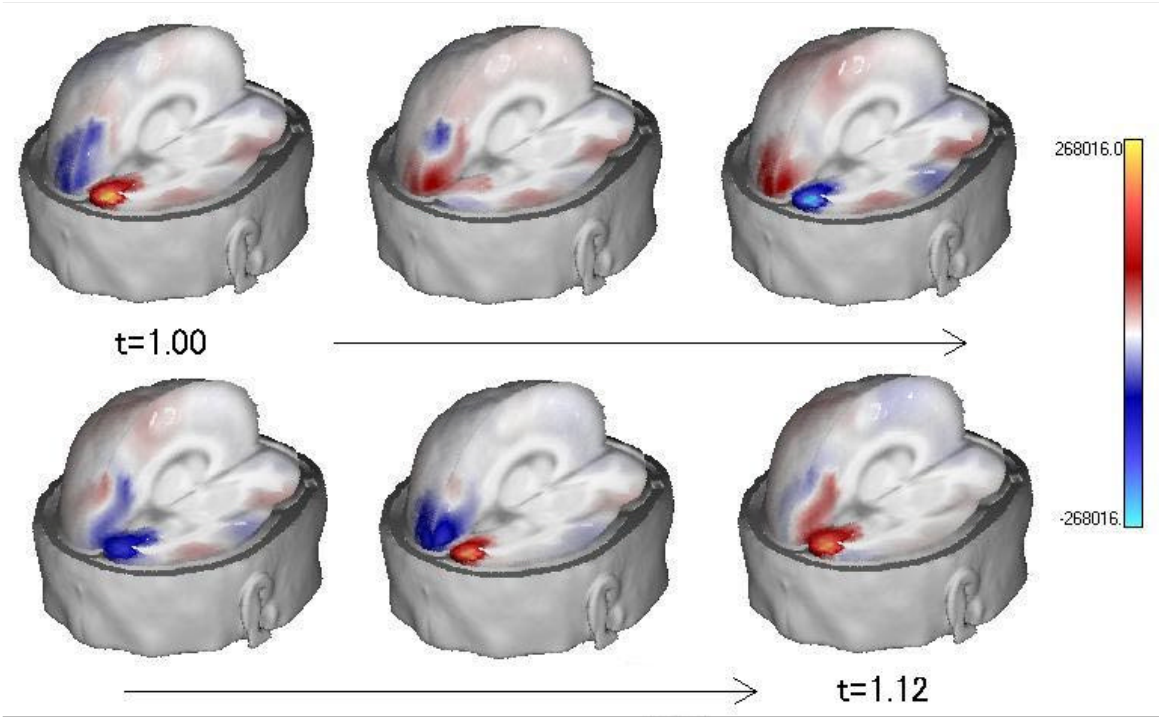
268016.0
-268016.
t=1.00
t=1.12

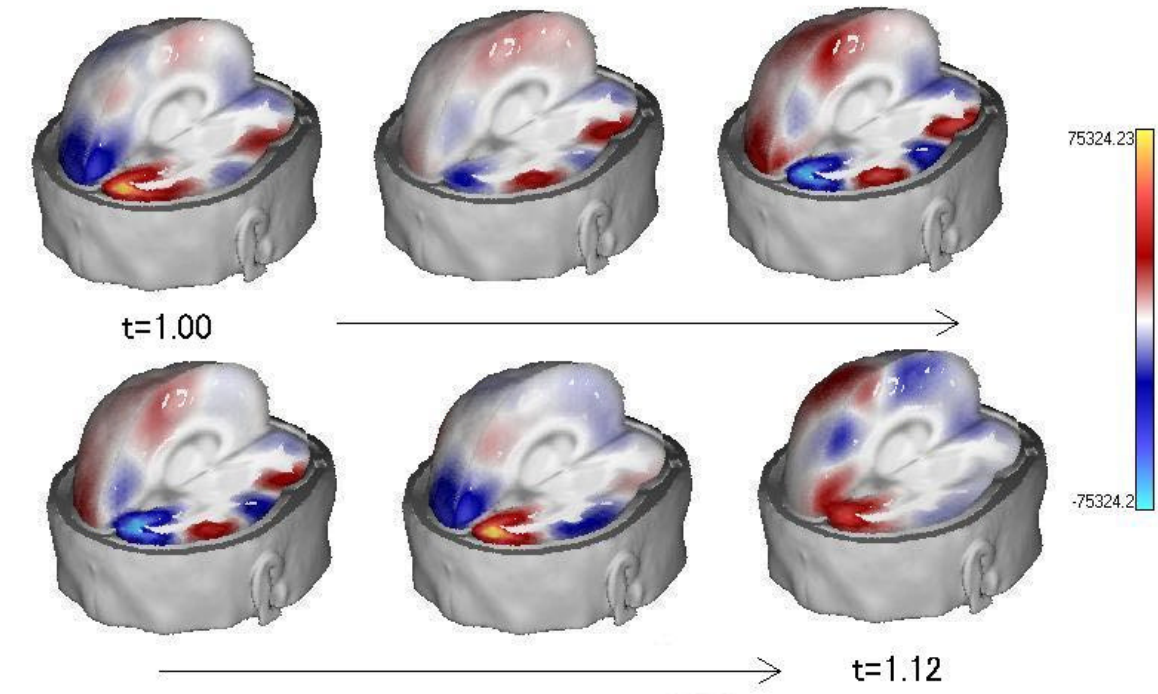
75324.23
-75324.2
t=1.00
t=1.12